Original Article

Institution of MECHANICAL ENGINEERS
Journal of MULTI-BODY DYNAMICS

Proc IMechE Part K:
J Multi-body Dynamics
0(0) 1–19

DOI: 10.1177/1464419318754647
journals.sagepub.com/home/pik
SAGE

Effect of integrated ride and cornering dynamics of a military vehicle on the weapon responses

Saayan Banerjee[1], Varadarajan Balamurugan[2] and R Krishna Kumar[3]

Abstract

The present study brings out the influence of a non-linear dynamics model of military vehicle with trailing arm suspension, on the weapon dynamics responses. A 20 degrees of freedom integrated ride and cornering dynamics model has sequentially been coupled with the 7 degrees of freedom weapon dynamics model. The 20 degrees of freedom integrated model includes the bounce, pitch, roll, longitudinal, lateral and yaw motions of the sprung mass and rotational dynamics of the 14 unsprung masses. The 7 degrees of freedom weapon model comprises the coupled elevation and azimuth dynamics. The coupled weapon model includes angular rotation of the elevation drive, breech and muzzle in elevation direction, as well as, angular rotation of the azimuth drive, turret, breech and muzzle in azimuth direction. The actual physical behaviour of each of the hydro-gas trailing arm suspension units is implemented in the governing differential equations. The non-linear governing equations also incorporate the dynamic coupling between each of the axle arms and sprung mass, which is an inherent behaviour of the trailing arm suspension, unlike their equivalent vertical representation. The integrated model has been simulated for different cornering manoeuvres at specified speeds. It is observed that the sprung mass dynamics, emanating from different manoeuvres, significantly affects the coupled elevation and azimuth dynamics responses of the weapon. The weapon dynamics model coupled with the integrated ride and cornering dynamics model of the military vehicle, would be useful for implementation of a suitable robust gun control system in military vehicles.

Keywords

Military vehicle, hydro-gas suspension, trailing arm dynamics, structural coupling, gun dynamics

Date received: 3 November 2017; accepted: 19 December 2017

Introduction

Military vehicles are designed to negotiate cross-country type of terrains with severe ground undulations. As the vehicle manoeuvres this type of terrain, stabilisation of the main gun, carried on these vehicles, becomes a challenge. Therefore, it is required to develop a coupled elevation and azimuth dynamics model of the weapon platform of military vehicle along with an integrated three-dimensional ride and cornering dynamics, in order to understand the weapon dynamic responses during various manoeuvres. The mathematical model for weapon elevation dynamics with an electric drive, has been developed using a lumped parameter flexible beam model, and integrated with an in-plane ride model of a full tracked vehicle.[1] A concise methodology for design of the gun barrel using both finite element techniques and lumped parameter flexible beam model has been evolved for standardising the problem, in both elevation as well as azimuth (traverse) drives.[2] The methodology of formulating the governing differential equations for the azimuth dynamics has been developed.[3] However, the influence of a three-dimensional vehicle dynamics response on the elevation and azimuth dynamics of the main gun, has not been brought out in the above studies. Moreover, the above studies do not consider influence of azimuth drive on the elevation dynamics of the gun. The theoretical analyses

[1]Center for Engineering Analysis and Design, Combat Vehicles R&D Estt., DRDO, Chennai, India
[2]Aircraft Projects Division, Combat Vehicles R&D Estt., DRDO, Chennai, India
[3]Department of Engineering Design, Indian Institute of Technology, Chennai, India

Corresponding author:
Saayan Banerjee, Center for Engineering Analysis and Design, Combat Vehicles R&D Establishment, DRDO, Chennai 600054, India.
Email: saayanbanerjee@cvrde.drdo.in

of non-stationary motion of a tracked vehicle have been carried out over level terrain, and steering dynamics has been formulated with a system of differential equations.[4] A multi-body dynamics model of the M113 Armoured Personal Carrier vehicle has been developed using LMS-DADS simulation software, with the objective of accurately predicting track dynamics.[5] The authors have carried out detailed studies on interaction between the track and terrain, and compared the simulation results with that of super-element track model, under various terrain and steering conditions.[5] Experimental studies are carried out on a miniature model of tracked vehicle running gear assembly, based on the suspension dynamics of challenger main battle tank (MBT).[6] The experimental results have been correlated with the predicted values from Waterways Experiment Station (WES) system of mobility numerics, and later implemented for future design of tracked vehicles.[6] The theoretical analysis has been carried out for predicting the steering dynamics of tracked vehicles, during uniform cornering manoeuvre on level pavement.[7] The authors have considered the effects of track slippage and vehicle configuration during formulation of the governing differential equations for steering.[7] A single station representation of military vehicle, incorporating the actual suspension kinematics, has been described, and sprung mass bounce dynamics response is successfully validated.[8] The inner and outer track forces for a military tracked vehicle has been estimated during skid-steer, and thereby, reasonable estimates for transmission loads have been obtained.[9] The author has considered variable tractive coefficient and pull-slip equations for formulating the prediction model of track forces.[9] A mathematical model of hydro-gas suspension unit (HSU) has been developed, incorporating fluid compressibility and expansion of other components, and thereafter, flow through damper valve is modeled through a look up table.[10] Ride quality of a six station vehicle is assessed by incorporating the HSU model.[10] The process of random road profile generation from temporal power spectral density (PSD) has been described.[11] In this model, the vehicle is considered to travel over the random terrain at a constant speed.[11] The non-linear ride dynamics model of the entire military vehicle has been formulated, and further validated with numerical experiments using MSC Adams.[12] The hydro-gas suspension characteristics are evaluated in an in-plane vehicle model, over sinusoidal terrains of various wavelengths and Aberdeen Proving Ground (APG).[13] The hydro-gas suspension spring characteristics are modelled using polytropic gas compression models, whereas damping orifices are modelled using hydraulic conductance.[13] An in-plane nonlinear computer simulation model of a high mobility tracked vehicle is described using Lagrangian model formulation.[14] Suspension dynamic analysis and ride quality assessment is carried out on an arbitrary rigid terrain with a constant vehicle speed, and experimentally evaluated on a discrete half round bump and random course.[14] A spatial motion analysis of tracked vehicles is carried out with torsion bar suspension systems for evaluation of ride, steerability and stability conditions on rough terrains.[15] The analysis was carried out using multi-body equations, in which separate equations of motions are initially formulated for the vehicle body, torsion bar arms, road-wheels and later coupled with constraint equations.[15] A mechanical model is developed, comprising three spatially and elastically supported bounded bodies, in which a new solution method for the equations of motion with higher degrees of freedom, is proposed.[16] A rail vehicle with elastic and dissipative members has been considered, in which, the vertical vibrations at any arbitrary position in the vehicle could be determined based on the above model.[16] A field test is conducted on a military tracked vehicle, in order to analyse the accelerations at selected locations on the vehicle for different types of terrains and different speed conditions.[17] A tracked vehicle having six bogie wheel stations, fitted with torsion bar suspension, has been considered for the analysis.[17] A finite element-based simulation model is described to investigate the vibration and ride dynamic characteristics of a medium weight, high-speed military tracked vehicle negotiating a non-deformable terrain.[18] Research is carried out to estimate the effect of suspension damping on vehicle ride.[19] A four degrees of freedom vehicle system is considered, in which the vibration differential equations and road excitation matrix were formulated and frequency response functions were obtained in order to evaluate the vehicle ride, based on the variation in shock absorber damping.[19] A simulation model is presented for predicting the transient longitudinal dynamics of a tracked vehicle.[20] The driving inputs in the model are estimated from a powertrain model, which includes the engine, transmission, torque converter and drivetrain.[20] However, the effect of coupling ride dynamics with the vehicle cornering dynamics, has not been brought out in the above studies.

It may be noted that even though there are number of research studies on military vehicle dynamics, no literature is available on developing the weapon dynamics, coupled with the integrated ride and cornering dynamics non-linear model of a full military vehicle with trailing arm suspension dynamics effects. The present work initially concentrates on development of the seven degrees of freedom coupled elevation and azimuth dynamics model of a weapon platform. Thereafter, non-linear ride model of the military vehicle, consisting of 17 degrees of freedom with hydro-gas suspension stiffness characteristics (described in Saayan Banerjee et al.[12]) are coupled through governing differential equations to additional 3 degrees of freedom (longitudinal, lateral and yaw dynamics), arising out of vehicle cornering behaviour; thereby forming a 20 degrees of freedom integrated

model. The model incorporates the trailing arm suspension dynamics of 14 wheel stations, coupled with bounce, pitch and roll motions of the sprung mass. The non-linear stiffness results from differential gas characteristics at each of the suspension stations. Each of the 14 wheel station inertias are coupled with the sprung mass inertias, which is an inherent behaviour of integrated trailing arm, unlike an equivalent vertical suspension. The track mass is lumped on each of the wheel stations, ignoring the track link dynamics. The responses from the weapon elevation and azimuth dynamics model are predicted, based on integrated vehicle dynamics inputs. Cornering events with differential track speeds and random terrain excitation are provided as inputs to the vehicle. The integrated model can later be used for implementing a robust gun control technique. The mathematical model is computationally effective, desired for a vehicle simulator, and also will play a key role in establishing an in-house dynamic simulation laboratory.

Development of weapon dynamics of the military vehicle

In the present section, weapon elevation and azimuth dynamics model are formulated. The main gun barrel will have its inherent degrees of freedom pertaining to both the elevation and azimuth drives, which in turn is sequentially coupled to the ride and cornering dynamics model. The main gun of the vehicle is driven in the elevation direction (YZ plane) and azimuth direction (XZ plane). The schematic diagram representing overall vehicle model with the integrated weapon platform (with all degrees of freedom indicated), is shown in Figure 1. The basic dimensional nomenclature for weapon dynamics is given in Figure 2(a).

Elevation and Azimuth dynamics model of the main gun

Based on literature, the coupled elevation and azimuth dynamics of the main gun are derived.[1,3] The main gun barrel is divided into muzzle and breech sections; and the model is based on lumped parameter flexible beam formulation. The elevation drive consists of an electric motor, providing required torque to elevate and depress the main gun barrel in vertical plane about the trunnion support. The elevation dynamics model consists of the rotational degrees of freedom about X axis, for the elevation drive 'θ_{de}', as well as 'θ_1' and 'θ_2' for the breech and muzzle sections, respectively, about their corresponding center of gravity (CG) locations. The elevation model also has vertical translational degrees of freedom 'y_1' and 'y_2' for the breech and muzzle sections along Y axis, respectively, measured at the corresponding CG locations. The elevation drive consists of a pinion, which is connected to

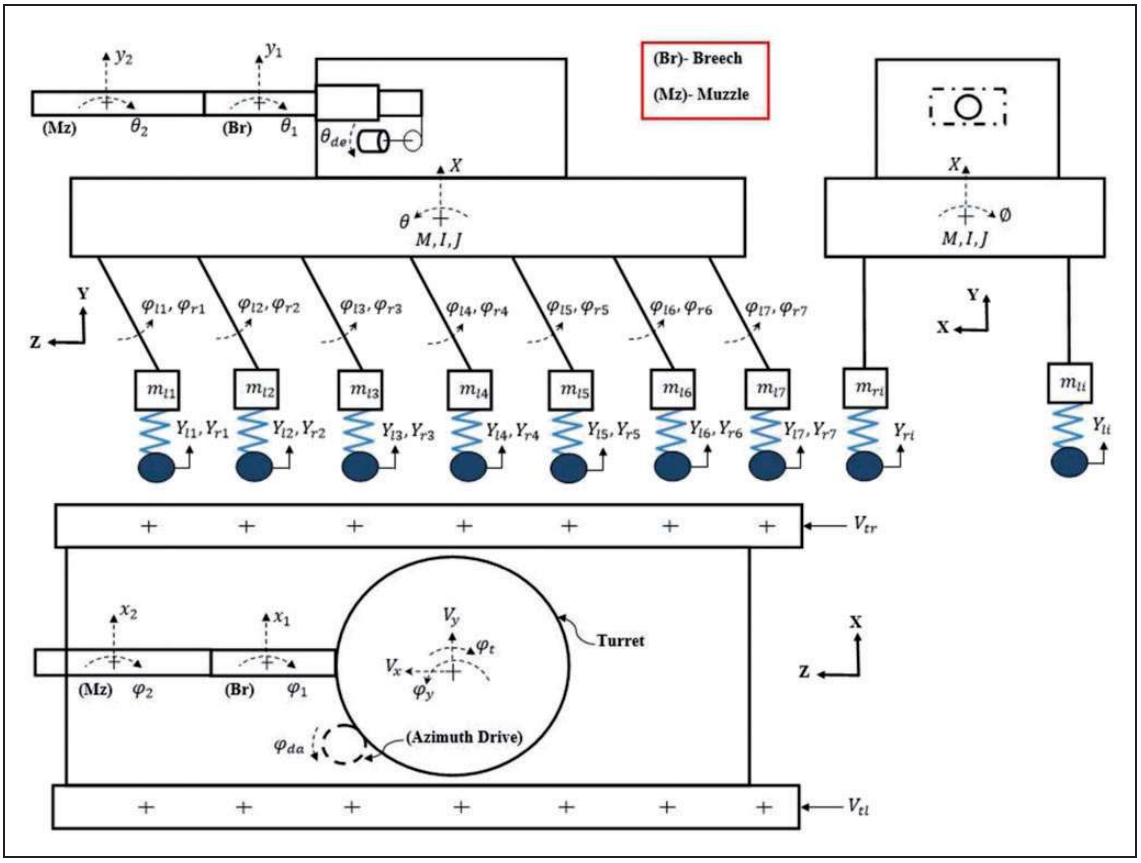

Figure 1. Schematic representation of the overall vehicle with integrated weapon platform (with all degrees of freedom indicated).

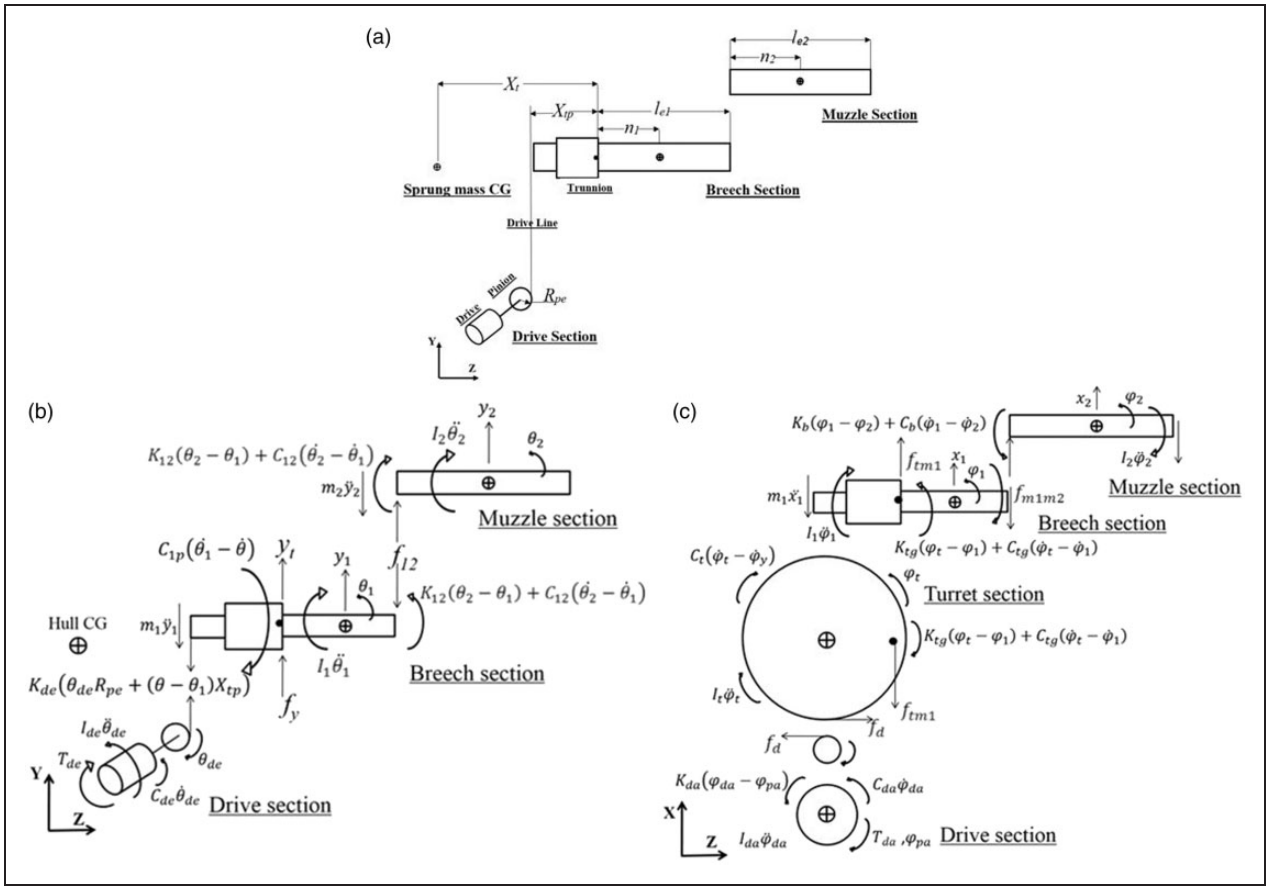

Figure 2. (a) Basic dimensional nomenclature for formulating the weapon dynamics. (b) Elevation dynamics in YZ plane. (c) Azimuth dynamics in XZ plane.

breech section with rack and pinion arrangement. The trunnion has a hinge joint, having torsional viscous damping characteristics. The breech and muzzle sections are connected together by hinge joint, having torsional stiffness and torsional viscous damping characteristics. The trunnion has vertical movement along Y axis. '$X(t)$', '$\theta(t)$' and '$\phi(t)$' represent the bounce, pitch and roll displacements at the vehicle sprung mass CG, respectively (as shown in Figure 3). The free body diagram for elevation dynamics is shown in Figure 2(b).

Apart from the elevation drive, the turret of the vehicle has an azimuth drive, which provides required torque to produce desired motion of the turret about Y axis. The main gun exhibits rotational motion about Y axis, by virtue of being connected to the turret at the trunnion. The azimuth dynamics model consists of rotational degree of freedom for azimuth drive section 'φ_{da}', as well as 'φ_t', 'φ_1' and 'φ_2', for the turret, breech and muzzle sections, respectively, about Y axis. The breech and muzzle sections also have lateral translational degrees of freedom 'x_1' and 'x_2', respectively, along X axis, measured at the corresponding CGs. The azimuth drive is coaxial with a pinion, which is meshed with the turret ring gear. Reaction force along Z axis, acts at the contact point between pinion and turret ring gear. The mounting interface between turret and hull is characterised by viscous torsional damping about Y axis. Apart from having torsional damping about X axis, the gun breech and turret are connected at the trunnion, having torsional stiffness and torsional viscous damping characteristics about Y axis. The trunnion has lateral movement along X axis. The connection interface between breech and muzzle has torsional stiffness and viscous damping characteristics about Y axis. 'K' and '$\dot{\varphi}_y(t)$' represent vehicle yaw moment of inertia and yaw velocity, about sprung mass CG (as shown in Figure 3). The free body diagram for azimuth dynamics is shown in Figure 2(c). The coupled governing differential equations of motion for the elevation and azimuth dynamics are derived, referring to Figure 2(c).

Equations of motion for the elevation dynamics

Rotational dynamics for the elevation drive. This is represented by equation (1).

$$I_{de}\ddot{\theta}_{de} - T_{de} + C_{de}\dot{\theta}_{de} + K_{de}\left(\theta_{de}R_{pe} + (\theta - \theta_1)X_{tp}\right)R_{pe} = 0 \quad (1)$$

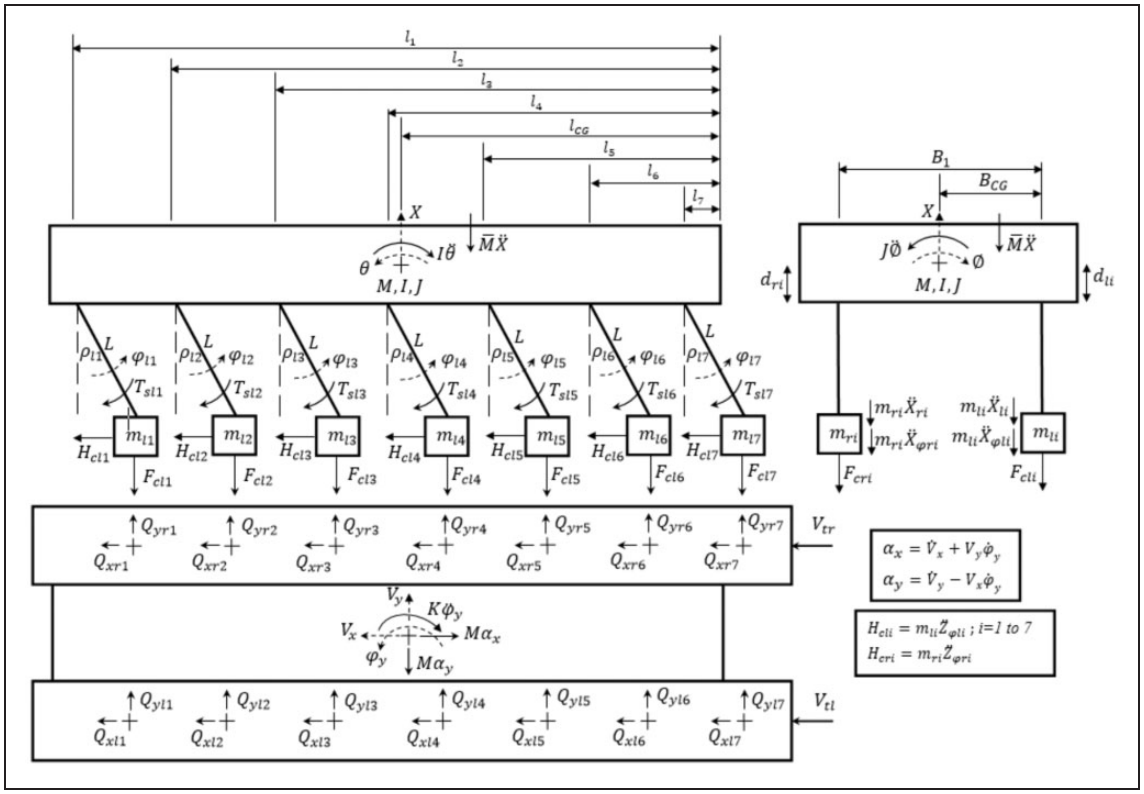

Figure 3. Representation of forces and moments for coupled vehicle dynamics model.

Vertical motion of gun breech section along Y axis. This is represented by equation (2).

$$m_1\ddot{y}_1 - f_y + K_{de}\left(\theta_{de}R_{pe} + (\theta - \theta_1)X_{tp}\right) + f_{12} = 0 \tag{2}$$

where

$$y_1 = y_t + \theta_1 n_1 - n_1\emptyset\sin(\varphi_t) \tag{3}$$

$$y_t = X + \theta X_t - X_t\emptyset\sin(\varphi_t) \tag{4}$$

Rotational motion of gun breech about X axis in the YZ plane. This is represented by equation (5).

$$\begin{aligned} &I_1\ddot{\theta}_1 + C_{1p}\left(\dot{\theta}_1 - \dot{\theta}\right) + f_{12}(l_{e1} - n_1) + f_y n_1 \\ &\quad - K_{12}(\theta_2 - \theta_1) - C_{12}\left(\dot{\theta}_2 - \dot{\theta}_1\right) \\ &\quad - K_{de}\left(\theta_{de}R_{pe} + (\theta - \theta_1)X_{tp}\right)\left(X_{tp} + n_1\right) = 0 \end{aligned} \tag{5}$$

Vertical motion of gun muzzle section along Y axis. This is represented by equation (6).

$$m_2\ddot{y}_2 - f_{12} = 0 \tag{6}$$

where

$$y_2 = y_t + \theta_2 n_2 + \theta_1 l_{e1} - (l_{e1} + n_2)\emptyset\sin(\varphi_t) \tag{7}$$

Rotational motion of gun muzzle section about X axis in the YZ plane. This is expressed in equation (8).

$$I_2\ddot{\theta}_2 + f_{12}n_2 + K_{12}(\theta_2 - \theta_1) + C_{12}\left(\dot{\theta}_2 - \dot{\theta}_1\right) = 0 \tag{8}$$

Equations of motion for the azimuth dynamics

Rotational motion of azimuth drive. This is expressed in equation (9).

$$I_{da}\ddot{\varphi}_{da} - T_{da} + K_{da}\left(\varphi_{da} - \varphi_{pa}\right) + C_{da}\dot{\varphi}_{da} = 0 \tag{9}$$

Equation of motion for pinion, meshed with turret. This is expressed in equation (10).

$$f_d R_{pa} = K_{da}\left(\varphi_{da} - \varphi_{pa}\right) \tag{10}$$

where

$$R_{pa}\varphi_{pa} = R_t\varphi_t \tag{11}$$

Rotational dynamics of turret about sprung mass CG in the XZ plane. This is expressed in equation (12).

$$\begin{aligned} &I_t\ddot{\varphi}_t - f_d R_t + C_t\left(\dot{\varphi}_t - \dot{\varphi}_y\right) + K_{tg}(\varphi_t - \varphi_1) \\ &\quad + C_{tg}(\dot{\varphi}_t - \dot{\varphi}_1) + f_{tm1}X_t - K\ddot{\varphi}_y = 0 \end{aligned} \tag{12}$$

Lateral motion of gun breech along X axis. This is expressed in equation (13).

$$m_1\ddot{x}_1 + f_{m1m2} - f_{tm1} = 0 \tag{13}$$

where

$$x_1 = x_{tr} + n_1\varphi_1 \tag{14}$$

$$x_{tr} = \bar{x} + X_t\left(\varphi_t + \varphi_y\right) \tag{15}$$

$\bar{x}$ = Lateral displacement of the vehicle, measured at sprung mass CG, along X axis.

φ_y = Yaw angular displacement of vehicle, about sprung mass CG, about Y axis.

Rotational dynamics of gun breech about Y axis in the XZ plane. This is expressed in equation (16).

$$\begin{aligned} &I_1\ddot{\varphi}_1 + K_b(\varphi_1 - \varphi_2) + C_b(\dot{\varphi}_1 - \dot{\varphi}_2) \\ &\quad + f_{tm1}n_1 + f_{m1m2}(l_{e1} - n_1) \\ &\quad - K_{tg}(\varphi_t - \varphi_1) - C_{tg}(\dot{\varphi}_t - \dot{\varphi}_1) = 0 \end{aligned} \tag{16}$$

Lateral motion of gun muzzle along X axis. This is expressed in equation (17).

$$m_2\ddot{x}_2 - f_{m1m2} = 0 \tag{17}$$

where

$$x_2 = x_{tr} + l_{e1}\varphi_1 + n_2\varphi_2 \tag{18}$$

Rotational motion of gun muzzle about Y axis in the XZ plane. This is expressed in equation (19).

$$I_2\ddot{\varphi}_2 - K_b(\varphi_1 - \varphi_2) - C_b(\dot{\varphi}_1 - \dot{\varphi}_2) + f_{m1m2}n_2 = 0 \tag{19}$$

Formulation of integrated ride and cornering dynamics model

The 17 degrees of freedom non-linear ride dynamics formulation of the military vehicle is described in detail.[12] In addition, the vehicle model contains longitudinal, lateral and yaw degrees of freedom, which pertains to cornering dynamics behaviour. The pure cornering dynamics of the military vehicle is initially formulated, based on the described methodology.[4] Thereafter, the vehicle ride degrees of freedom are coupled with cornering degrees of freedom, thereby forming a 20 degrees of freedom integrated ride and cornering non-linear model. The coupled governing differential equations are derived for 20 degrees of freedom of the vehicle, namely sprung mass bounce, pitch and roll motions, vehicle longitudinal, lateral and yaw motions, as well as rotational dynamics for each of the 14 unsprung masses. The coordinate system, followed for three-dimensional force and moment representation of the entire vehicle, is highlighted in Figure 3. The nomenclatures of various parameters (as indicated in Figure 3) pertaining to the vehicle ride model, are already described.[12] Remaining parameters are described subsequently. Due to relative longitudinal and lateral motions of the vehicle, slip takes place between each of the road–wheel springs and ground. '$\varepsilon_{li}(t)$' and '$\varepsilon_{ri}(t)$' represent slip under left and right roadwheel springs ($i = 1$–7), as shown by equations (20) and (21), respectively.

$$\varepsilon_{li} = atan(V_{yli}/V_{xli}) \tag{20}$$

$$\varepsilon_{ri} = atan(V_{yri}/V_{xri}) \tag{21}$$

where

$$V_{xli} = V_x - B_{CG}\dot{\varphi}_y - V_{tl} \tag{22}$$

$$V_{xri} = V_x + (B_1 - B_{CG})\dot{\varphi}_y - V_{tr} \tag{23}$$

$$V_{yli} = V_y - D_{li}\dot{\varphi}_y \qquad [D_{li} = l_i - l_{CG} - Lsin(\rho_{li})] \tag{24}$$

$$V_{yri} = V_y - D_{ri}\dot{\varphi}_y \qquad [D_{ri} = l_i - l_{CG} - Lsin(\rho_{ri})] \tag{25}$$

The friction forces are determined from the net dynamic vertical reaction forces on each of the road-wheel springs, as well as from slips between the road-wheel springs and ground. Separate coupled non-linear governing differential equations of motion are developed for the vehicle, referring to Figure 3.

Bounce motion of sprung mass from the integrated dynamics model

The vertical bounce motion contains inertia coupling effect due to vertical inertia of the sprung mass as well as vertical inertia of unsprung masses, resulting from unsprung mass rotational motion.[12] Bounce dynamics of the sprung mass also incorporates the effects, produced from cornering motion, and additionally couples with the longitudinal, lateral and yaw dynamics of the vehicle. The forces, resulting from road–wheel spring deflections, are also contributed from cornering behaviour of the vehicle, and in turn affects the overall bounce response, expressed in equation (26) as

$$\begin{aligned} &M\ddot{X} + \sum_{i=1}^{7} m_{li}(\ddot{X}_{li} + \ddot{X}_{\varphi li}) \\ &\quad + \sum_{i=1}^{7} m_{ri}(\ddot{X}_{ri} + \ddot{X}_{\varphi ri}) + \sum_{i=1}^{7} F_{cli} + \sum_{i=1}^{7} F_{cri} = 0 \end{aligned} \tag{26}$$

where, F_{cli} and F_{cri} are the vertical restoring forces from the roadwheel translational springs, belonging to left and right side *ith* suspension stations respectively ($i = 1$–7), measured at unsprung mass CG, due to the coupled effect from both ride and cornering dynamics.

$$F_{cli} = k_{tli}\left[X_{li} + X_{\varphi li} + X_{li\_ax} - X_{li\_ay} - Y_{li}\right] \tag{27}$$

$$F_{cri} = k_{tri}\left[X_{ri} + X_{\varphi ri} + X_{ri\_ax} + X_{ri\_ay} - Y_{ri}\right] \tag{28}$$

X_{li_ax} and X_{ri_ax} are the dynamic deflections of roadwheel translational springs, belonging to left and right side *ith* suspension stations, respectively ($i = 1$–7), resulting from moments due to vehicle longitudinal acceleration, about the road–wheel centre.

$$X_{li\_ax} = \frac{M(B_1 - B_{CG})D_{li}}{B_1 \sum_{i=1}^{7} k_{tli} D_{li}^2} \quad (\dot{V}_x + V_y\dot{\varphi}_y)\,(H + X) \tag{29}$$

$$X_{ri\_ax} = \frac{MB_{CG}D_{ri}}{B_1 \sum_{i=1}^{7} k_{tri} D_{ri}^2} \quad (\dot{V}_x + V_y\dot{\varphi}_y)\,(H + X) \tag{30}$$

$$\bar{M} = M + \sum_{i=1}^{7} m_{li} + \sum_{i=1}^{7} m_{ri} \tag{31}$$

X_{li_ay} and X_{ri_ay} are the dynamic deflections of roadwheel translational springs, belonging to left and right side *ith* suspension stations, respectively ($i = 1$–7), resulting from moments due to vehicle lateral acceleration, about the road–wheel centre.

$$X_{ri\_ay} = \frac{M\,(B_1 - B_{CG})}{7\{k_{tr1}B_{CG}^2 + k_{tr2}(B_1 - B_{CG})^2\}} \times (\dot{V}_y - V_x\dot{\varphi}_y)\,(H + X) \tag{32}$$

$$X_{li\_ay} = \frac{M\,B_{CG}}{7\{k_{tl1}B_{CG}^2 + k_{tl2}(B_1 - B_{CG})^2\}} \times (\dot{V}_y - V_x\dot{\varphi}_y)\,(H + X) \tag{33}$$

Pitch motion of sprung mass from the integrated dynamics model

The longitudinal friction forces between roadwheel spring and ground, resulting from dynamic reaction forces due to longitudinal and lateral inertias, also affect the vehicle pitch response, apart from the effects due to ride-induced degrees of freedom. The pitch dynamics about the sprung mass CG is written in equation (34) as

$$\begin{aligned} I\ddot{\theta} &- \sum_{i=1}^{7} m_{li}(\ddot{X}_{li} + \ddot{X}_{\varphi li})D_{li} - \sum_{i=1}^{7} m_{ri}(\ddot{X}_{ri} + \ddot{X}_{\varphi ri})D_{ri} \\ &+ \sum_{i=1}^{7} m_{li}\ddot{Z}_{\varphi li}L_{\varphi li} + \sum_{i=1}^{7} m_{ri}\ddot{Z}_{\varphi ri}L_{\varphi ri} \\ &- \sum_{i=1}^{7} F_{cli}D_{li} - \sum_{i=1}^{7} F_{cri}D_{ri} + \sum_{i=1}^{7} P_{xli} + \sum_{i=1}^{7} P_{xri} = 0 \end{aligned} \tag{34}$$

where, $m_{li}\ddot{Z}_{\varphi li}L_{\varphi li}$ is the pitching moment about sprung mass CG, due to horizontal component of rotational inertia ($m_{li}\ddot{Y}_{\varphi li}$) and longitudinal inertia ($m_{li}\alpha_{xli}$) of the left *ith* wheel station ($i = 1$–7).

$$\ddot{Z}_{\varphi li} = \ddot{Y}_{\varphi li} - \alpha_{xli} \tag{35}$$

$$\alpha_{xli} = \dot{V}_{xli} + V_{yli}\dot{\varphi}_y \tag{36}$$

$m_{ri}\ddot{Z}_{\varphi ri}L_{\varphi ri}$ is the pitching moment about sprung mass CG, due to horizontal component of rotational inertia ($m_{ri}\ddot{Y}_{\varphi ri}$) and longitudinal inertia ($m_{ri}\alpha_{xri}$) of the right *ith* wheel station ($i = 1$–7).

$$\ddot{Z}_{\varphi ri} = \ddot{Y}_{\varphi ri} - \alpha_{xri} \tag{37}$$

$$\alpha_{xri} = \dot{V}_{xri} + V_{yri}\dot{\varphi}_y \tag{38}$$

$F_{cli}D_{li}$ and $F_{cri}D_{li}$ are the pitching moments about sprung mass CG due to vertical restoring force from roadwheel translational springs, belonging to left and right side *ith* suspension stations respectively ($i = 1$–7).

P_{xli} and P_{xri} are the moments about sprung mass CG, due to longitudinal friction forces between roadwheel springs and ground, belonging to left and right side *ith* suspension stations respectively ($i = 1$–7).

$$P_{xli} = Q_{xli}\,L_{\varphi li} \tag{39}$$

$$P_{xri} = Q_{xri}\,L_{\varphi ri} \tag{40}$$

$$Q_{xli} = \mu_x \cos(\pi + \varepsilon_{li})k_{tli}x_{tli} - \mu_x \cos(\pi + \varepsilon_{li})F_{cli} \tag{41}$$

$$Q_{xri} = \mu_x \cos(\pi + \varepsilon_{ri})k_{tri}x_{tri} - \mu_x \cos(\pi + \varepsilon_{ri})F_{cri} \tag{42}$$

x_{tli} and x_{tri} are the static deflections on left and right roadwheel springs ($i = 1$–7).[12]

Roll motion of the sprung mass due to the coupled ride and cornering dynamics

The roll motion of sprung mass is affected by rotational dynamics of the suspension. Apart from that, lateral friction forces between roadwheel springs and ground, resulting from dynamic reaction forces due to longitudinal and lateral inertias, also affect the sprung mass roll response. The sprung mass roll motion about CG is expressed in equation (43) as

$$\begin{aligned} J\ddot{\emptyset} &- \sum_{i=1}^{7} m_{li}(\ddot{X}_{li} + \ddot{X}_{\varphi li})\,B_{CG} + \sum_{i=1}^{7} m_{ri}(\ddot{X}_{ri} + \ddot{X}_{\varphi ri})B_2 \\ &+ \sum_{i=1}^{7} m_{li}\alpha_{yli}L_{\varphi li} + \sum_{i=1}^{7} m_{ri}\alpha_{yri}L_{\varphi ri} - \sum_{i=1}^{7} F_{cli}B_{CG} \\ &+ \sum_{i=1}^{7} F_{cri}B_2 - \sum_{i=1}^{7} P_{yli} - \sum_{i=1}^{7} P_{yri} = 0 \end{aligned} \tag{43}$$

where $B_2 = B_1 - B_{CG}$.

$m_{li}\alpha_{yli}L_{\varphi li}$ is the rolling moment about sprung mass CG, due to lateral inertia ($m_{li}\alpha_{yli}$) of the left *ith* wheel station ($i = 1$–7).

$$\alpha_{yli} = \dot{V}_{yli} - V_{xli}\dot{\varphi}_y \tag{44}$$

$m_{ri}\alpha_{yri}L_{\varphi ri}$ is the rolling moment about sprung mass CG, due to lateral inertia ($m_{ri}\alpha_{yri}$) of the right *ith* wheel station ($i = 1$–7).

$$\alpha_{yri} = \dot{V}_{yri} - V_{xli}\dot{\varphi}_y \tag{45}$$

$F_{cli}B_{CG}$ and $F_{cri}B_2$ are the rolling moments about sprung mass CG, due to vertical restoring forces from the roadwheel translational springs, belonging to left and right side *ith* suspension stations, respectively ($i = 1$–7).

P_{yli} and P_{yri} are the moments about sprung mass CG, due to lateral friction forces between roadwheel springs and ground, belonging to left and right side *ith* suspension stations respectively ($i = 1$–7).

$$P_{yli} = Q_{yli}\, L_{\varphi li} \tag{46}$$

$$P_{yri} = Q_{yri}\, L_{\varphi ri} \tag{47}$$

$$Q_{yli} = \mu_y \sin(\pi + \varepsilon_{li})k_{tli}x_{tli} - \mu_y \sin(\pi + \varepsilon_{li})F_{cli} \tag{48}$$

$$Q_{yri} = \mu_y \sin(\pi + \varepsilon_{ri})k_{tri}x_{tri} - \mu_y \sin(\pi + \varepsilon_{ri})F_{cri} \tag{49}$$

Angular rotational motion of left and right side unsprung masses measured about pivot location of corresponding axle arm, due to integrated dynamics

Angular motion of the unsprung mass also includes inertia coupling effect due to rotational inertia of unsprung mass and unsprung mass translation, resulting from sprung mass motion. The angular dynamics is further affected by longitudinal inertia effects. The angular motion of each of the left and right side unsprung masses, measured about the axle arm pivot locations, is expressed in equations (50) and (51) as

$$\begin{aligned} &m_{li}L^2\ddot{\varphi}_{li} + m_{li}\ddot{X}_{li}Lsin(\rho_{li} + \varphi_{li}) \\ &\quad - m_{li}\alpha_{xli}Lcos(\rho_{li} + \varphi_{li}) \\ &\quad + \ (T_{li} - T_{stli}) + c\dot{x}_{li}L_o + \ F_{cli}Lsin(\rho_{li} + \varphi_{li}) = 0 \end{aligned} \tag{50}$$

$$\begin{aligned} &m_{ri}L^2\ddot{\varphi}_{ri} + m_{ri}\ddot{X}_{ri}Lsin(\rho_{ri} + \varphi_{ri}) \\ &\quad - m_{ri}\alpha_{xri}Lcos(\rho_{ri} + \varphi_{ri}) \\ &\quad + \ (T_{ri} - T_{stri}) + c\dot{x}_{ri}L_o + \ F_{cri}Lsin(\rho_{ri} + \varphi_{ri}) = 0 \end{aligned} \tag{51}$$

Longitudinal motion of the vehicle due to coupled ride and cornering dynamics

Longitudinal forces on the vehicle are equilibrated by dynamic longitudinal friction forces between roadwheel springs and ground, for all wheel stations. The longitudinal motion is additionally affected by rotational dynamics of trailing arm suspension. The vehicle longitudinal motion at sprung mass CG is expressed in equation (52) as

$$\begin{aligned} &M\left(\dot{V}_x + V_y\dot{\varphi}_y\right) + \sum_{i=1}^{7} m_{li}\alpha_{xli} \ + \sum_{i=1}^{7} m_{ri}\alpha_{xri} \\ &\quad - \sum_{i=1}^{7} m_{li}\ddot{Y}_{\varphi li} - \sum_{i=1}^{7} m_{ri}\ddot{Y}_{\varphi ri} - \sum_{i=1}^{7} Q_{xli} - \sum_{i=1}^{7} Q_{xri} = 0 \end{aligned} \tag{52}$$

Lateral motion of the vehicle as a result of the integrated dynamics

Lateral forces on the vehicle are equilibrated by dynamic lateral friction forces between roadwheel springs and ground, for all wheel stations. The vehicle lateral motion at sprung mass CG is written in equation (53) as

$$\begin{aligned} &M\left(\dot{V}_y - V_x\dot{\varphi}_y\right) + \sum_{i=1}^{7} m_{li}\alpha_{yli} \\ &\quad + \sum_{i=1}^{7} m_{ri}\alpha_{yri} \ - \sum_{i=1}^{7} Q_{yli} - \sum_{i=1}^{7} Q_{yri} = 0 \end{aligned} \tag{53}$$

Yaw motion of the vehicle pertaining to the coupled dynamics

Yaw motion of the vehicle is equilibrated by moments about sprung mass CG, produced due to generated longitudinal and lateral friction forces between roadwheel springs and ground. The vehicle yaw motion about sprung mass CG is written in equation (54) as

$$\begin{aligned} &K\ddot{\varphi}_y + \sum_{i=1}^{7} Q_{yli}\, D_{li} \ + \sum_{i=1}^{7} Q_{yri}\, D_{ri} + \sum_{i=1}^{7} Q_{xli}B_{CG} \\ &\quad - \sum_{i=1}^{7} Q_{xri}B_2 \ - \sum_{i=1}^{7} m_{li}\alpha_{yli}D_{li} - \sum_{i=1}^{7} m_{ri}\alpha_{yri}D_{ri} \\ &\quad + \sum_{i=1}^{7} m_{li}\ddot{Z}_{\varphi li}B_{CG} - \sum_{i=1}^{7} m_{ri}\ddot{Z}_{\varphi ri}B_2 = 0 \end{aligned} \tag{54}$$

Solution of the coupled vehicle dynamics model

Equations (20) to (54) are coded in Matlab. Second-order differential equations are formulated for sprung mass bounce, pitch, roll dynamics and unsprung mass

rotational dynamics for each of the 14 unsprung masses; whereas, first-order differential equations are formulated for the vehicle longitudinal, lateral and yaw dynamics. Therefore, the second-order equations are reduced to first-order form and thereafter, the system of 20 first-order differential equations are numerically simulated with explicit time integration procedures. The differential track speed input and input base displacements, corresponding to various terrain excitations, are modeled in Simulink using signal builder approach. Cubic interpolation technique is used to interpolate the base excitation inputs and differential track velocities over different times. The Matlab code is synchronized with Simulink signal builder to appropriately extract the inputs.

Solution of the weapon dynamics model

The terms 'f_y' and 'f_{12}', being unknown forces, are eliminated from equations (2) and (6). Similarly, forces 'f_d', 'f_{tm1}' and 'f_{m1m2}' are also eliminated from equations (10), (13) and (17). The displacement terms, 'y_1', 'y_2', 'x_1' and 'x_2' are replaced by substitutions from equations (3), (4), (7), (14), (15) and (18), respectively, in the corresponding equations of motion. Therefore, the coupled elevation and azimuth dynamics model of the weapon system, reduces to a seven degrees of freedom non-linear model, which are subsequently coded in Matlab using non-linear state space approach (described in Appendix 1). The 7 degrees of freedom weapon dynamics model has sequentially been coupled to the 20 degrees of freedom ride and cornering dynamics model of the entire vehicle. The system of equations is numerically simulated with explicit time-integration procedures. The drive torques, differential track speed input and input base displacements are modeled in Simulink using signal builder approach. The solution procedure is similar as that, described in previous section.

Prediction of weapon dynamics behaviour from coupled vehicle dynamics

The integrated ride and cornering dynamics model are simulated over the random terrain at vehicle speed of 40 kmph, as well as over plain terrain with differential track speed inputs varying from 20 to 15 kmph on both left hand (LH) and right hand (RH) sides. In the above simulations, the lateral and longitudinal dynamic friction coefficients between roadwheel springs and ground are assumed as 0.5. It may be noted that there is no separate tyre model used in the above simulations, as the military vehicle is considered to have a track system, wrapped around. Therefore, the road–wheel springs comprise the solid tyre and bottom track pad stiffness. Due to combined motion of the vehicle, the

Table 1. Magnitudes of various parameters for a military vehicle.

Parameter	Magnitude
M, Sprung mass	75,000 kg
I, Pitch moment of inertia of the sprung mass about CG	5.3×10^5 kgm^2
J, Roll moment of inertia of the sprung mass about CG	8×10^4 kgm^2
m_{li} and m_{ri}, Left and right *ith* unsprung masses ($i = 1$–7)	575.5 kg
k_{tli} and k_{tri}, Left and right *ith* roadwheel stiffness ($i = 1$–7)	8000 kN/m
L, Axle arm length of each suspension station	0.55 m
L_0, Perpendicular distance between actuator piston axis and pivot	0.137 m
l_1, Distance between first suspension pivot and vehicle end	5.44 m
l_2, Distance between second suspension pivot and vehicle end	4.65 m
l_3, Distance between third suspension pivot and vehicle end	3.80 m
l_4, Distance between fourth suspension pivot and vehicle end	2.96 m
l_5, Distance between fifth suspension pivot and vehicle end	2.12 m
l_6, Distance between sixth suspension pivot and vehicle end	1.31 m
l_7, Distance between seventh suspension pivot and vehicle end	0.50 m
l_{CG}, Distance between sprung mass CG and vehicle end	2.67 m
B_1, Distance between left and right side suspension stations	2.25 m
B_{CG}, Distance between left suspensions and sprung mass CG	1.125 m
α_{li} and α_{ri}, Angle between the axle arm of left and right *ith* suspension stations and vertical direction, at rebound position	20.36° ($i = 1$) 32° ($i = 2$–7)
d_{li} and d_{ri}, Vertical distance between left and right *ith* suspension stations and sprung mass CG ($i = 1$–7)	0.25 m ($i = 1$) 0.3 m ($1 = 2$–7)
c, Suspension viscous damping coefficient, along the cylinder axis	400 kNs/m
Charging pressures at first, second, sixth and seventh left and right stations	11.4 MPa
Charging pressures at third, fourth and fifth stations	10.7 MPa

road–wheel springs will have both longitudinal and lateral velocities. By virtue of the road–wheel longitudinal and lateral motions, lateral slip occurs between the bottom track pads and ground. Longitudinal and lateral friction forces between the road–wheel spring and ground, are estimated from the respective slips, dynamic friction coefficients and net vertical forces on the respective road–wheel springs, as highlighted in equations (41), (42), (48) and (49), respectively. The dynamics friction coefficients will vary based on nature of the terrain. The longitudinal and lateral friction forces can accordingly be estimated in the computational domain from the above equations. The parametric values used in the vehicle dynamics and weapon dynamics models are described in Tables 1 and 2, respectively.

Gun dynamics analysis over random terrain with variance of 0.064 m^2 at 40 kmph

The coupled vehicle dynamics model is subjected to random terrain excitation with variance of 0.064 m^2, at 40 kmph speed. The elevation torque is initially applied as pulse input for 5 s with peak value of 1000 Nm, followed by similar pattern of azimuth drive torque provided from the 7th s with peak value of 2000 Nm (shown in Figure 4). The vehicle is stationary till both drive torques are applied. After that, the vehicle is accelerated from rest to a speed of 40 kmph in 18 s, with both LH and RH tracks maintained at the same speed (shown in Figure 4). The base excitation is applied from the 40th s to the corresponding road wheels, simulating vehicle movement over random terrain. The total simulation is carried out for 90 s.

Figure 5 represents the sprung mass CG bounce displacement as well as breech and muzzle angular displacement responses in the elevation direction, respectively in time domain. The PSD for sprung mass CG bounce acceleration and muzzle angular acceleration in the elevation direction is indicated in Figure 6.

The initial torque is applied to the azimuth and elevation drives in order to position the gun barrel at a particular orientation, followed by subsequent movement over the terrain. From Figure 5, variations are observed in breech and muzzle angular dynamics

Table 2. Magnitudes of various parameters for weapon dynamics.

Parameter	Magnitude
X_t, Distance between sprung mass CG and trunnion	1 m
X_{tp}, Distance between trunnion and elevation pinion centre	0.75 m
K_{de}, Elevation driveline stiffness	6000 kN/m
C_{de}, Elevation driveline torsional viscous damping coefficient	1.5 kNms/rad
R_{pe}, Elevation pinion radius	0.04 m
I_{de}, Elevation drive mass moment of inertia	0.5 kg m^2
C_{1p}, Torsional viscous damping coefficient at trunnion in elevation	1.5 kNms/rad
m_1, Gun breech section mass	2165 kg
I_1, Gun breech mass moment of inertia, measured about breech CG	1090 kgm^2
l_{e1}, Length of the gun breech section, measured from the trunnion	1.75 m
n_1, Distance between breech CG and trunnion	0.465 m
K_{12}, Torsional stiffness between breech and muzzle, about X axis	4000 kNm/rad
C_{12}, Torsional viscous damping coefficient between breech and muzzle, about X axis	2 kNms/rad
m_2, Gun muzzle section mass	335 kg
I_2, Gun muzzle mass moment of inertia, about muzzle CG	281 kgm^2
l_{e2}, Length of the gun muzzle section	3.25 m
n_2, Distance between muzzle CG and connection interface between breech and muzzle	1.32 m
I_{da}, Mass moment of inertia of azimuth drive gear	25 kgm^2
K_{da}, Driveline stiffness of azimuth drive	2000 kNm/rad
C_{da}, Torsional viscous damping coefficient of azimuth drive	150 kNms/rad
R_t, Turret ring gear pitch circle radius	1.1 m
R_{pa}, Azimuth pinion pitch circle radius	0.08 m
I_t, Mass moment of inertia of turret about sprung mass CG	1.6×10^5 kgm^2
C_t, Torsional viscous damping coefficient at connection interface between turret and hull	90 kNms/rad
K_{tg}, Torsional stiffness between turret and gun about Y axis	4.5×10^5 kNm/rad
C_{tg}, Torsional viscous damping coefficient between turret and gun about Y axis	225 kNms/rad
K_b, Torsional stiffness between breech and muzzle, about Y axis	4000 kNm/rad
C_b, Torsional viscous damping coefficient between breech and muzzle about Y axis	2 kNms/rad

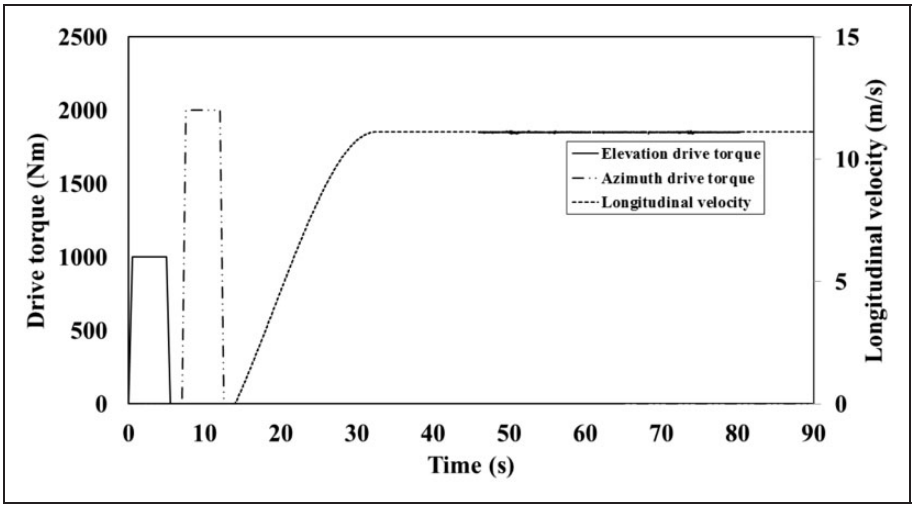

Figure 4. Variation of elevation and azimuth torques as well as longitudinal velocity.

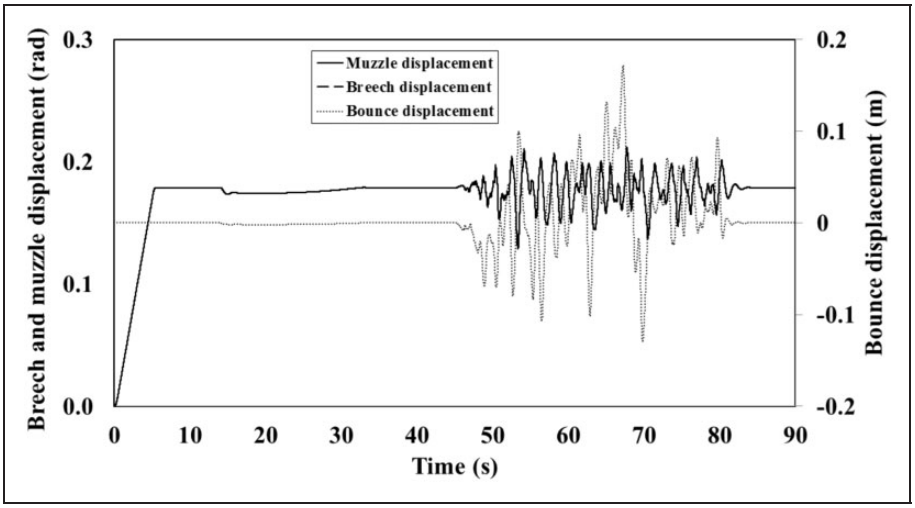

Figure 5. Variation of breech and muzzle elevation angular displacements as well as bounce displacement with time, over random terrain at 40 kmph.

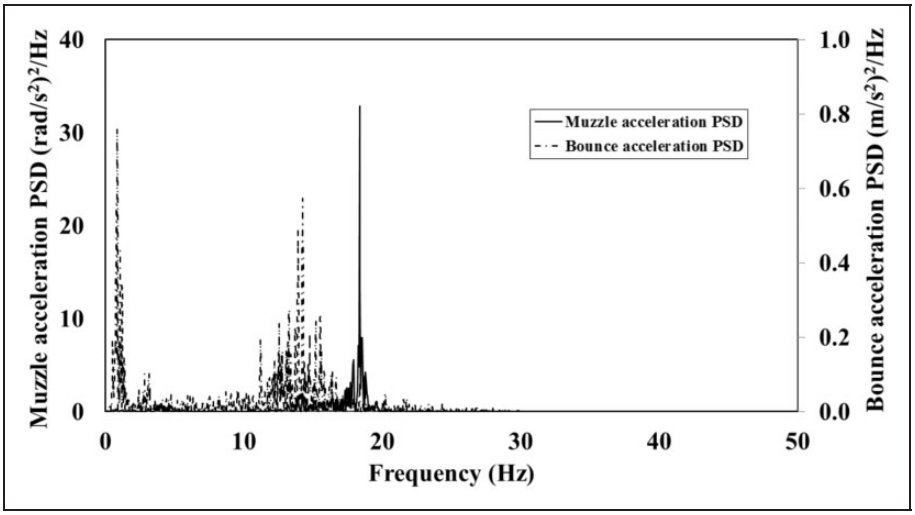

Figure 6. Variation of muzzle and bounce accelerations in frequency domain, over random terrain at 40 kmph.

over the random terrain. From Figure 6, peak magnitudes of muzzle angular acceleration PSD in the elevation direction occur at about 18 Hz, which is close to the natural frequency of the weapon system. As the vehicle almost moves in a straight path, the lateral and yaw angular velocity magnitudes are negligible, and therefore, its influence on gun azimuth motion is insignificant.

Estimation of gun dynamics over plain terrain with differential speeds of 20 and 15 kmph

The integrated vehicle model is also simulated over plain terrain with differential track speed inputs of 20 and 15 kmph. Keeping the vehicle stationary, the drive torque inputs are applied in similar manner, as described in the previous section. Thereafter, the vehicle is accelerated from rest to a speed of 20 kmph in 16 s, with both tracks maintained at same speed (shown in Figure 7). From the 40th s, cyclic variation of track speed is provided to both LH and RH tracks from 15 to 20 kmph (shown in Figure 7). The model is simulated for a total time of 140 s.

Figure 8 represents the sprung mass CG bounce displacement as well as pitch and roll angular displacement responses about CG, respectively. Figure 9 represents the breech and muzzle angular displacement responses in elevation direction. The yaw velocity, turret, breech and muzzle displacements in azimuth, are highlighted in Figure 10.

Unlike previous section, the present case study highlights the influence of vehicle cornering behaviour on the weapon azimuth dynamics as well. During the manoeuvre, the yaw velocity is significant enough to affect the azimuth response of the gun (observed from Figure 10). There is close similarity in turret, breech and

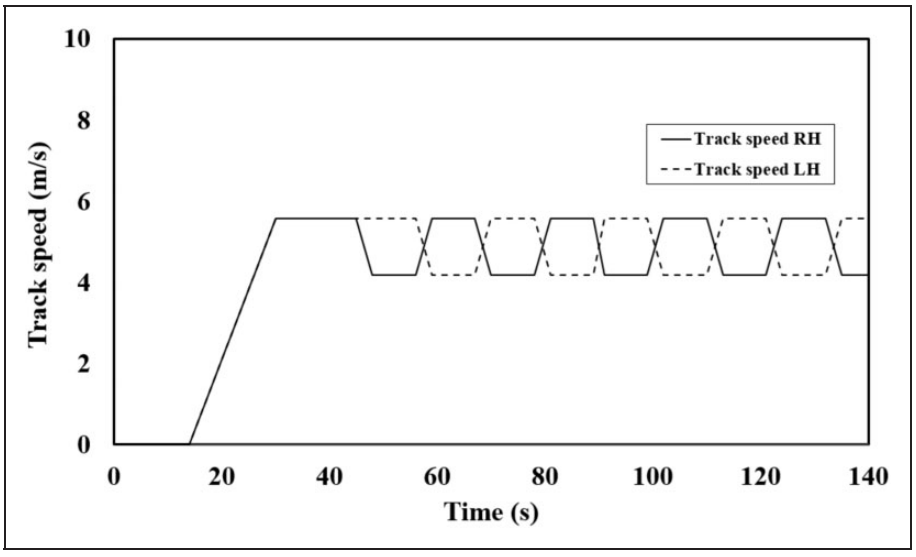

Figure 7. Variation of differential track speed with time.

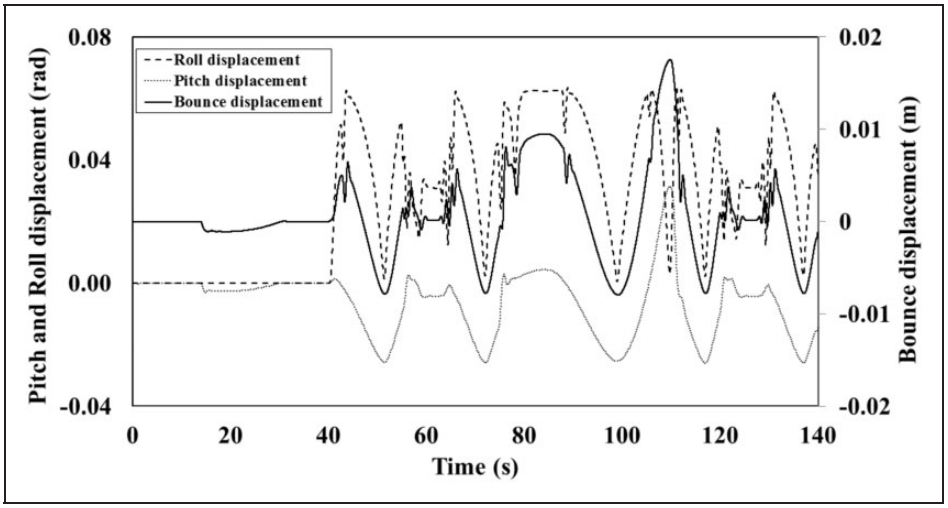

Figure 8. Variation of sprung mass bounce, pitch and roll displacements in time domain, with differential track speed variation between 15 and 20 kmph.

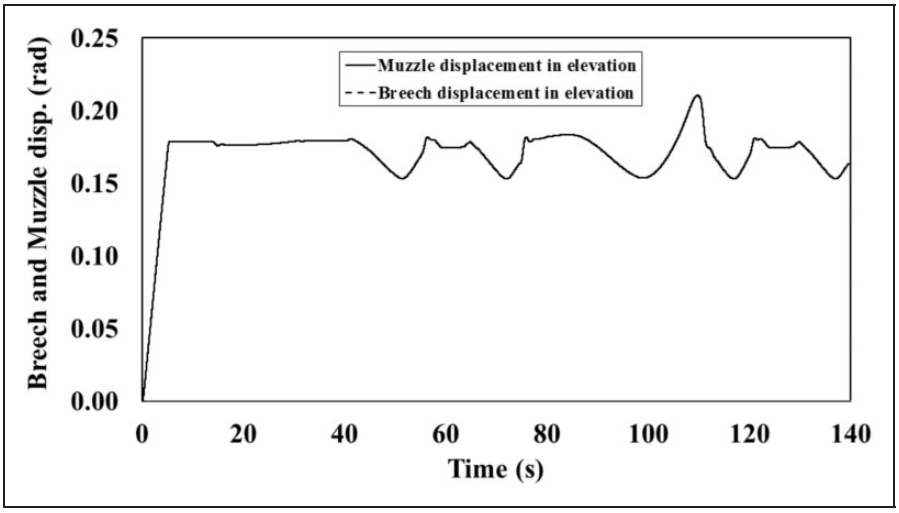

Figure 9. Variation of muzzle and breech elevation angular displacements in time domain, with differential track speed variation between 15 and 20 kmph.

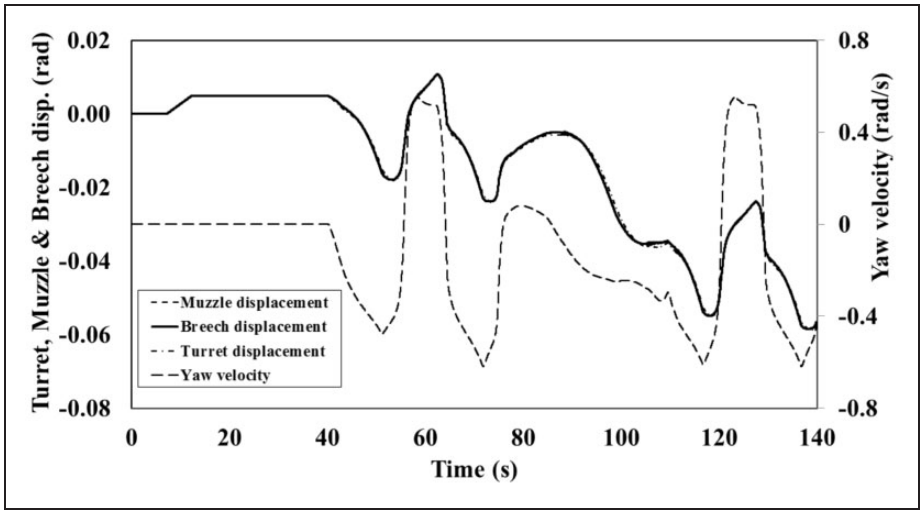

Figure 10. Variation of turret, muzzle and breech azimuth angular displacements as well as yaw velocity in time domain, with track speed variation between 15 and 20 kmph.

muzzle azimuth angular responses. In this case, though there is no base excitation, still there is a variation of breech and muzzle response in elevation direction, by virtue of the coupled weapon dynamics model.

Conclusion

The present study highlights a novel approach to development of a sequentially coupled weapon dynamics and vehicle dynamics model, with the effect of trailing arm hydro-gas suspension. The proposed mathematical ride, cornering and weapon dynamics model is a generic one and may be used for any military vehicle with trailing arm suspensions. The model has superior computational benefits over the commercially available multi-body dynamics software tools. It is observed that the sprung mass dynamics significantly affects the structural dynamics responses of the weapon platform in elevation and azimuth directions, over different manoeuvring environments. The natural frequencies of the weapon model reside within the sprung mass frequency spectrum over the random terrain, which is an unavoidable phenomenon. The dynamics influence of the azimuth responses on the elevation model is also observed during the cornering manoeuvres. This study is an essential pre-requisite for developing robust gun controllers for military vehicles. This study can form a platform for implementation of suitable gun control algorithms and deciding the location of control actuators. The model can be used for parametric evaluation of ride dynamics and fine tuning the suspension characteristics for improving the vehicle ride comfort, as well as for capturing the dynamics over different cornering manoeuvres. The model can easily be implemented in a military vehicle simulator. The coupled model can also be used to predict the vehicle dynamics during gun firing. The developed

integrated vehicle dynamics model would be a very useful design platform for freezing the suspension configuration of future military vehicles.

Acknowledgements

The authors are grateful to Dr. P. Sivakumar, Director, CVRDE and Shri. S. Ramesh, Addl. Director (CEAD) for extending all required facilities to carry out the research.

Declaration of Conflicting Interests

The author(s) declared no potential conflicts of interest with respect to the research, authorship and/or publication of this paper.

Funding

The author(s) received no financial support for the research, authorship, and/or publication of this article.

References

1. Purdy DJ. Comparison of balance and out of balance main battle tank armaments. *Shock Vibrat* 2001; 8: 167–174.
2. Dholiwar DK. *Control of out of balance servo-mechanisms subjected to external disturbances*. PhD Thesis, Loughborough University, USA, 2007.
3. Karamayuk T. *Modeling and stabilisation control of a main battle tank*, PhD Thesis, Middle East Technical University, Turkey, 2011.
4. Kitano M and Kuma M. An analysis of horizontal plane motion of tracked vehicles. *J Terramech* 1977; 14: 211–225.
5. Rubinstein R and Hitron R. A detailed multi-body model for dynamic simulation of off-road tracked vehicles. *J Terramech* 2004; 41: 163–173.
6. Hetherington J. Tracked vehicle operations on sand- investigations at model scale. *J Terramech* 2005; 42: 65–70.
7. Kitano M and Jyozaki H. A theoretical analysis of steeribility of tracked vehicles. *J Terramech* 1976; 13: 241–258.
8. Banerjee S, Balamurugan V and Krishnakumar R. Ride dynamics mathematical model for a single station representation of tracked vehicle. *J Terramech* 2014; 53: 47–58.
9. Kar M. Prediction of track forces in skid-steering of military tracked vehicles. *J Terramech* 1987; 24: 75–86.
10. Purdy J and Rajesh Kumar J. Mathematical modeling of hydro gas suspension unit for tracked military vehicles. *J Battlefield Technol* 2005; 8: 7–14.
11. Tyan F, Hong Y-F, Tu S-H, et al. Generation of random road profiles. *J Adv Eng* 2009; 4: 151–156.
12. Banerjee S, Balamurugan V and Krishnakumar R. Ride comfort analysis of math ride dynamics model of full tracked vehicle with trailing arm suspension. *J Proced Eng* 2016; 144: 1110–1118.
13. Solomon U and Padmanabhan C. Hydro-gas suspension system for a tracked vehicle: modeling and analysis. *J Terramech* 2011; 48: 125–137.
14. Dhir A and Sankar S. Assessment of tracked vehicle suspension system using a validated computer simulation model. *J Terramech* 1995; 32: 127–149.
15. Yamakawa J and Watanabe K. A spatial motion analysis model of tracked vehicles with torsion bar type suspension. *J Terramech* 2004; 41: 113–126.
16. Soukup J, Skocilas J and Skocilasova B. Vertical vibration of the vehicle model with higher degree of freedom. *Proced Eng* 2014; 96: 435–443.
17. Sujatha C, Goswami AK and Roopchand J. Vibration and ride comfort studies on a tracked vehicle. *Int J Heavy Vehicle Syst* 2002; 9: 241–252.
18. Balamurugan V. Dynamic analysis of a military tracked vehicle. *Def Sci J* 2000; 50: 155–165.
19. XuiMei S, Chu Y, Fan J, et al. Research of simulation on the effect of suspension damping on vehicle ride. *Energy Proced* 2012; 17: 145–151.
20. Janarthanan B, Padmanabhan C and Sujatha C. Longitudinal dynamics of a tracked vehicle: simulation and experiment. *J Terramech* 2012; 49: 63–72.

Appendix

Notation

$A(\emptyset, \varphi_t)$	non-linear system matrix (for state space formulation of coupled elevation and azimuth dynamics)
B_1	distance between left and right suspension stations
B_2	difference between B_1 and B_{CG}
B_{CG}	distance between left-side suspension stations and sprung mass CG
$B(X, \theta, V_y,$ $\varphi_y, T_{de}, T_{da})$	non-linear input matrix (for state space formulation of coupled elevation and azimuth dynamics)
c	viscous damping coefficient of the suspension, along the direction of actuator piston motion in line with the cylinder axis (for single station)
C_b	torsional viscous damping about Y axis, at the connection interface between breech and muzzle sections
C_{da}	torsional viscous damping coefficient in the azimuth drive
C_{de}	torsional viscous damping in the elevation drive
C_{1p}	torsional viscous damping coefficient of trunnion hinge about X axis
C_t	torsional viscous damping coefficient at the mounting interface between turret and hull, about Y axis
C_{tg}	torsional viscous damping about Y axis, at the trunnion interface, connecting the gun breech section and turret
C_{12}	torsional viscous damping at the connection interface between breech and muzzle, about X axis
d_{li} , d_{ri}	distance between axle arm pivot points of left and right side *ith* suspensions and sprung mass CG, measured vertically ($i = 1$–7)
D_{li} , D_{ri}	horizontal distance between points of support of left and right *ith* ($i = 1$–7) suspensions on ground, from

sprung mass CG, during axle arm rotation from static equilibrium condition

F_{cli} , F_{cri} vertical restoring forces from tyre and track pad translational springs, belonging to left and rights side *ith* suspension stations respectively ($i = 1$–7), measured at unsprung mass CG, due to the coupled effect from both ride and cornering dynamics

f_d reaction force at the point of contact between pinion and turret ring gear, measured along Z direction

f_{m1m2} lateral reaction force along X axis, at the connection interface between breech and muzzle sections

f_{tm1} lateral reaction force along X axis, at the trunnion interface, connecting the gun breech section and turret

f_y vertical reaction force on the trunnion hinge along Y axis

f_{12} vertical reaction force at the connection interface between breech and muzzle sections, along Y axis

H distance between the sprung mass CG and road–wheel tyre center, measured vertically, after vehicle attains static equilibrium

I pitch moment of inertia of the sprung mass about CG

I_{da} mass moment of inertia for the azimuth drive

I_{de} mass moment of inertia for the elevation drive

I_1 mass moment of inertia of breech section about its CG

I_2 mass moment of inertia of muzzle section about its CG

I_t mass moment of inertia of the turret about sprung mass CG

J roll moment of inertia of the sprung mass about CG

K vehicle yaw moment of inertia about sprung mass CG

K_b torsional stiffness about Y axis, at the connection interface between breech and muzzle sections

K_{da} torsional stiffness of the azimuth drive

K_{de} driveline stiffness of rack and pinion arrangement for elevation drive

K_{tg} torsional stiffness about Y axis, at the trunnion interface, connecting the gun breech section and turret

k_{tli} , k_{tri} equivalent translational stiffness of road-wheel with track pads, belonging to left and right side *ith* suspension stations. ($i = 1$–7)

K_{12} torsional stiffness at the connection interface between breech and muzzle, about X axis

L length of the axle arm

l_{CG} longitudinal distance between sprung mass CG and vehicle end

l_{e1} length of breech section

l_{e2} length of the muzzle section

l_i longitudinal distance between pivot points of left and right *ith* ($i = 1$–7) suspension stations and the vehicle end

L_o perpendicular distance between the actuator piston axis and pivot point

$L_{\varphi li}$, $L_{\varphi ri}$ vertical distance between the left and right *ith* road–wheel center and axle arm pivot location, respectively ($i = 1$–7)

M sprung mass

$\bar{M}$ summation of the sprung mass and all the unsprung masses

m_{li} , m_{ri} left and right *ith* unsprung masses ($i = 1$–7)

m_1 mass of breech section

m_2 mass of muzzle section

$\hat{M}(\emptyset, \varphi_t)$ non-linear mass matrix (for state space formulation of coupled elevation and azimuth dynamics)

n_1 distance between breech section CG and trunnion

n_2 distance between muzzle section CG and hinge, located between breech and muzzle sections

P_{xli} , P_{xri} moments due to longitudinal friction forces between the track-pad and ground, belonging to left and right side *ith* suspension stations respectively ($i = 1$–7), about the sprung mass CG

P_{yli} , P_{yri} moments due to lateral friction forces between the track-pad and ground, belonging to left and right side *ith* suspension stations respectively ($i = 1$–7), about the sprung mass CG

Q_{xli} , Q_{xri} longitudinal friction forces, acting between the bottom of left and right side *ith* tyre springs and ground ($i = 1$–7)

Q_{yli} , Q_{yri} lateral friction forces, acting between the bottom of left and right side *ith* tyre springs and ground ($i = 1$–7)

R_{pa} Pinion radius, corresponding to azimuth drive

R_{pe} Pinion radius for the elevation drive

R_t radius of turret ring gear, corresponding to azimuth drive

T_{da} torque required for azimuth rotation of the turret about Y axis

T_{de} torque required to elevate and depress the main gun barrel

T_{li} , T_{ri} moments about axle arm rotational axis, from left and right side *ith* ($i = 1$–7) suspension gas spring restoring forces on actuator piston, during trailing arm rotation from static position

T_{stli} , T_{stri} static reaction moments on left and right *ith* ($i = 1$–7) suspension stations about respective pivot points (for full military vehicle)

$V_{tl}(t)$ longitudinal track velocity on ground, resulting from sprocket motion, on left side of the vehicle

$V_{tr}(t)$ longitudinal track velocity on ground, resulting from sprocket motion, on right side of the vehicle

$V_x(t)$ longitudinal velocity at sprung mass CG

$V_{xli}(t)$ relative longitudinal velocity, measured below the left *ith* tyre and track pad springs ($i = 1$–7)

$V_{xri}(t)$ relative longitudinal velocity, measured below the right *ith* tyre and track pad springs ($i = 1$–7)

$V_y(t)$ lateral velocity at sprung mass CG

$V_{yli}(t)$ relative lateral velocity, measured below the left *ith* tyre and track pad springs ($i = 1$–7)

$V_{yri}(t)$ relative lateral velocity, measured below the right *ith* tyre and track pad springs ($i = 1$–7)

x_{li} , x_{ri} actuator piston displacement of left and right side *ith* ($i = 1$–7) suspensions, measured in line with the actuator cylinder axis, from static equilibrium position

x_{tli} , x_{tri} static deflection of the left and right *ith* road–wheel tyre springs of the full military vehicle ($i = 1$–7)

x_{tr} lateral displacement at the trunnion along X axis

x_1 , x_2 lateral translational degrees of freedom for muzzle and breech sections along X axis

$\bar{x}$ lateral displacement of the vehicle, at sprung mass CG, along X axis.

$X(t)$ bounce displacement of sprung mass, measured from static position

X_{li} , X_{ri} vertical translational displacement of left and right *ith* wheel stations ($i = 1$–7) respectively, due to coupled bounce, pitch and roll motion of sprung mass about CG

X_{li_ax} , X_{ri_ax} dynamic deflections of tyre and track pad translational springs, belonging to left and right side *ith* suspension stations respectively ($i = 1$–7), resulting from moments due to vehicle longitudinal acceleration about the tyre centre

X_{li_ay} , X_{ri_ay} dynamic deflections of tyre and track pad translational springs, belonging to left and right side *ith* suspension stations respectively ($i = 1$–7), resulting from moments due to vehicle lateral acceleration about the tyre centre

X_t distance between trunnion and sprung mass CG

X_{tp} distance between trunnion and pinion centre

$X_{\varphi li}$, $X_{\varphi ri}$ vertical displacement component due to rotational motion of the left and right *ith* wheel stations ($i = 1$–7) respectively

y_1 , y_2 vertical translational degrees of freedom for the breech and muzzle sections along Y axis, respectively

y_t vertical displacement of the trunnion along Y axis

$Y(t)$ base excitation from the terrain (for single station)

$Y_{li}(t)$ base excitation at tyre spring bottom of left *ith* suspension ($i = 1$–7)

$Y_{ri}(t)$ base excitation at tyre spring bottom of right *ith* suspension ($i = 1$–7)

$Y_{\varphi li}$, $Y_{\varphi ri}$ horizontal displacement component due to rotational motion of the left and right *ith* wheel stations ($i = 1$–7) respectively

Z state vector (for state space formulation of coupled elevation and azimuth dynamics)

$\ddot{Z}_{\varphi li}$, $\ddot{Z}_{\varphi ri}$ difference between the horizontal component of rotational acceleration and longitudinal acceleration, pertaining to left and right side *ith* suspension stations respectively ($i = 1$–7)

α_{xli} , α_{xri} longitudinal acceleration of the left and right *ith* suspension stations, respectively ($i = 1$–7)

α_{yli} , α_{yri} lateral acceleration of the left and right *ith* suspension stations, respectively ($i = 1$–7)

$\varepsilon_{li}(t)$ slip under the left *ith* tyre and track-pad spring, resulting from longitudinal and lateral motion of the vehicle ($i = 1$–7)

$\varepsilon_{ri}(t)$ slip under the right *ith* tyre and track-pad spring, resulting from longitudinal and lateral motion of the vehicle ($i = 1$–7)

θ_{de} rotational degree of freedom for the elevation drive about X axis

θ_1	rotational degree of freedom for the breech section about X axis
θ_2	rotational degree of freedom for the muzzle section about X axis
$\theta(t)$	pitch angular displacement of sprung mass, from stationary position
μ_x , μ_y	longitudinal and lateral dynamic coefficients of friction between tyre as well as track-pad springs and ground, for all wheel stations
$\rho_{li}(t)$	angle between the left *ith* unsprung mass static settlement position and vertical direction ($i = 1$–7)
$\rho_{ri}(t)$	angle between the right *ith* unsprung mass static settlement position and vertical direction ($i = 1$–7)
φ_{da}	rotational degree of freedom for azimuth drive about Y axis
φ_t	rotational degree of freedom for turret about Y axis
φ_1 , φ_2	rotational degree of freedom for muzzle and breech about Y axis
φ_{pa}	rotational angle for turret pinion about Y axis
$\varphi_{li}(t)$	relative angular displacement of the left side *ith* unsprung mass, with respect to sprung mass, from stationary position ($i = 1$–7)
$\varphi_{ri}(t)$	relative angular displacement of the right side *ith* unsprung mass, with respect to sprung mass, from stationary position ($i = 1$–7)
$\phi(t)$	roll angular displacement of sprung mass, from stationary position
$\varphi_y(t)$	yaw angular rotation about sprung mass CG

Appendix I

If

$$\begin{aligned}\dot{\theta}_{de} &= p1\\ \dot{\theta}_1 &= p2\\ \dot{\theta}_2 &= p3\\ \dot{\varphi}_{da} &= p4\\ \dot{\varphi}_t &= p5\\ \dot{\varphi}_1 &= p6\\ \dot{\varphi}_2 &= p7\end{aligned}$$

Substituting $\dot{\theta}_{de}$, $\dot{\theta}_1$, $\dot{\theta}_2$, $\dot{\varphi}_{da}$, $\dot{\varphi}_t$, $\dot{\varphi}_1$ and $\dot{\varphi}_2$ in equations (1) to (19) and thereafter converting the equations to matrix domain

$$\dot{Z} = \frac{1}{\hat{M}(\emptyset, \varphi_t)}\left\{A(\emptyset, \varphi_t)Z + B(X, \theta, V_y, \varphi_y, T_{de},\ T_{da})\right\} \tag{55}$$

where,

$$Z = \begin{bmatrix} p1\\ p2\\ p3\\ p4\\ p5\\ p6\\ p7\\ \theta_{de}\\ \theta_1\\ \theta_2\\ \varphi_{da}\\ \varphi_t\\ \varphi_1\\ \varphi_2 \end{bmatrix}$$

$$\hat{M}(\emptyset,\varphi_t)=\begin{bmatrix} M11 & 0 & 0 & 0 & 0 & 0 & 0 & 0 & 0 & 0 & 0 & 0 & 0 & 0\\ 0 & M22 & M23 & 0 & M25 & 0 & 0 & 0 & 0 & 0 & 0 & 0 & 0 & 0\\ 0 & M32 & M33 & 0 & M35 & 0 & 0 & 0 & 0 & 0 & 0 & 0 & 0 & 0\\ 0 & 0 & 0 & M44 & 0 & 0 & 0 & 0 & 0 & 0 & 0 & 0 & 0 & 0\\ 0 & 0 & 0 & 0 & M55 & M56 & M57 & 0 & 0 & 0 & 0 & 0 & 0 & 0\\ 0 & 0 & 0 & 0 & M65 & M66 & M67 & 0 & 0 & 0 & 0 & 0 & 0 & 0\\ 0 & 0 & 0 & 0 & M75 & M76 & M77 & 0 & 0 & 0 & 0 & 0 & 0 & 0\\ 0 & 0 & 0 & 0 & 0 & 0 & 0 & 1 & 0 & 0 & 0 & 0 & 0 & 0\\ 0 & 0 & 0 & 0 & 0 & 0 & 0 & 0 & 1 & 0 & 0 & 0 & 0 & 0\\ 0 & 0 & 0 & 0 & 0 & 0 & 0 & 0 & 0 & 1 & 0 & 0 & 0 & 0\\ 0 & 0 & 0 & 0 & 0 & 0 & 0 & 0 & 0 & 0 & 1 & 0 & 0 & 0\\ 0 & 0 & 0 & 0 & 0 & 0 & 0 & 0 & 0 & 0 & 0 & 1 & 0 & 0\\ 0 & 0 & 0 & 0 & 0 & 0 & 0 & 0 & 0 & 0 & 0 & 0 & 1 & 0\\ 0 & 0 & 0 & 0 & 0 & 0 & 0 & 0 & 0 & 0 & 0 & 0 & 0 & 1 \end{bmatrix}$$

$$A(\emptyset,\varphi_t)=\begin{bmatrix} A11 & 0 & 0 & 0 & 0 & 0 & 0 & A18 & A19 & 0 & 0 & 0 & 0 & 0\\ 0 & A22 & A23 & 0 & A25 & 0 & 0 & A28 & A29 & A210 & 0 & A212 & 0 & 0\\ 0 & A32 & A33 & 0 & A35 & 0 & 0 & 0 & A39 & A310 & 0 & A312 & 0 & 0\\ 0 & 0 & 0 & A44 & 0 & 0 & 0 & 0 & 0 & 0 & A411 & A412 & 0 & 0\\ 0 & 0 & 0 & 0 & A55 & A56 & 0 & 0 & 0 & 0 & A511 & A512 & A513 & 0\\ 0 & 0 & 0 & 0 & A65 & A66 & A67 & 0 & 0 & 0 & 0 & A612 & A613 & A614\\ 0 & 0 & 0 & 0 & 0 & A76 & A77 & 0 & 0 & 0 & 0 & 0 & A713 & A714\\ 1 & 0 & 0 & 0 & 0 & 0 & 0 & 0 & 0 & 0 & 0 & 0 & 0 & 0\\ 0 & 1 & 0 & 0 & 0 & 0 & 0 & 0 & 0 & 0 & 0 & 0 & 0 & 0\\ 0 & 0 & 1 & 0 & 0 & 0 & 0 & 0 & 0 & 0 & 0 & 0 & 0 & 0\\ 0 & 0 & 0 & 1 & 0 & 0 & 0 & 0 & 0 & 0 & 0 & 0 & 0 & 0\\ 0 & 0 & 0 & 0 & 1 & 0 & 0 & 0 & 0 & 0 & 0 & 0 & 0 & 0\\ 0 & 0 & 0 & 0 & 0 & 1 & 0 & 0 & 0 & 0 & 0 & 0 & 0 & 0\\ 0 & 0 & 0 & 0 & 0 & 0 & 1 & 0 & 0 & 0 & 0 & 0 & 0 & 0 \end{bmatrix}$$

$$B(X,\theta,V_y,\varphi_y,T_{de},\ T_{da})=\begin{bmatrix} B11\\ B21\\ B31\\ B41\\ B51\\ B61\\ B71\\ 0\\ 0\\ 0\\ 0\\ 0\\ 0\\ 0 \end{bmatrix}$$

Elements inside the matrix $\hat{M}(\emptyset,\varphi_t)$ are described as follows

$$M11 = I_{de}$$

$$M22 = I_1 + m_1 n_1^2 + m_2 le_1^2$$

$$M23 = m_2 le_1 n_2$$

$$M25 = -\left\{m_1 n_1 (X_t + n_1) + m_2 le_1 (X_t + le_1 + n_2)\right\} \times \emptyset\cos(\varphi_t)$$

$$M32 = m_2 n_2 le_1$$

$$M33 = I_2 + m_2 n_2^2$$

$$M35 = -m_2 n_2 (X_t + n_2 + le_1)\ \emptyset\cos(\varphi_t)$$

$$M44 = I_{da}$$

$$M55 = I_t + m_1 X_t^2 + m_2 X_t^2$$

$$M56 = m_1 n_1 X_t + m_2 X_t le_1$$

$$M57 = m_2 X_t n_2$$

$$M65 = m_1 n_1 X_t + m_2 X_t le_1$$

$$M66 = I_1 + m_1 n_1^2 + m_2 le_1^2$$

$$M67 = m_2 n_2 le_1$$

$$M75 = m_2 X_t n_2$$
$$M76 = m_2 n_2 le_1$$
$$M77 = I_2 + m_2 n_2^2$$

Elements inside the matrix $A(\emptyset, \varphi_t)$ are described as follows

$$A11 = -C_{de}$$
$$A18 = -K_{de} R_{pe}^2$$
$$A19 = K_{de} X_{tp} R_{pe}$$
$$A22 = -C_{1p} - C_{12}$$
$$A23 = C_{12}$$
$$A25 = \left\{m_1 n_1 (X_t + n_1) + m_2 le_1 (X_t + le_1 + n_2)\right\} \times \left\{2\dot{\emptyset}\cos(\varphi_t) - \emptyset \overset{\sin}{\dot{\varphi}_t}(\varphi_t)\right\}$$
$$A28 = K_{de} X_{tp} R_{pe}$$
$$A29 = -K_{de} X_{tp}^2 - K_{12}$$
$$A210 = K_{12}$$
$$A212 = \left\{m_1 n_1 (X_t + n_1) + m_2 le_1 (X_t + le_1 + n_2)\right\} \ddot{\emptyset} \times \left\{1 - \frac{\varphi_t^2}{6} + \frac{\varphi_t^4}{120}\right\}$$
$$A32 = C_{12}$$
$$A33 = -C_{12}$$
$$A35 = m_2 n_2 (X_t + le_1 + n_2) \dot{\varphi}_t \times \left\{2\dot{\emptyset}\cos(\varphi_t) - \emptyset \sin(\varphi_t)\right\}$$
$$A39 = K_{12}$$
$$A310 = -K_{12}$$
$$A312 = m_2 n_2 (X_t + le_1 + n_2) \ddot{\emptyset} \left\{1 - \frac{\varphi_t^2}{6} + \frac{\varphi_t^4}{120}\right\}$$
$$A44 = -C_{da}$$
$$A411 = -K_{da}$$
$$A412 = \frac{K_{da} R_t}{R_{pa}}$$
$$A55 = -C_t - C_{tg}$$
$$A56 = C_{tg}$$
$$A511 = \frac{K_{da} R_t}{R_{pa}}$$
$$A512 = -\left(K_{tg} + \frac{K_{da} R_t^2}{R_{pa}^2}\right)$$
$$A513 = K_{tg}$$
$$A65 = C_{tg}$$
$$A66 = -C_b - C_{tg}$$
$$A67 = C_b$$
$$A612 = K_{tg}$$
$$A613 = -K_b - K_{tg}$$
$$A614 = K_b$$
$$A76 = C_b$$
$$A77 = -C_b$$
$$A713 = K_b$$
$$A714 = -K_b$$

Elements inside the matrix $B(X, \theta, V_y, \varphi_y, T_{de}, T_{da})$ are described as follows

$$B11 = T_{de} - K_{de} X_{tp} R_{pe} \theta$$
$$B21 = -(m_1 n_1 + m_2 le_1)\left\{\ddot{X} + X_t \ddot{\theta}\right\} + K_{de} X_{tp}^2 \theta + C_{12} \dot{\theta}$$
$$B31 = -m_2 n_2 \left\{\ddot{X} + X_t \ddot{\theta}\right\}$$
$$B41 = T_{da}$$
$$B51 = C_t \dot{\varphi}_y + \left(K - m_1 X_t^2 - n_2 X_t^2\right) \ddot{\varphi}_y - (m_1 X_t + m_2 X_t) \dot{V}_y$$
$$B61 = -(m_1 n_1 X_t + m_2 le_1 X_t) \ddot{\varphi}_y - (m_1 n_1 + m_2 le_1) \dot{V}_y$$
$$B71 = -m_2 n_2 X_t \ddot{\varphi}_y - m_2 n_2 \dot{V}_y$$

As observed from equation (55), the matrices $\hat{M}(\emptyset, \varphi_t)$ and $A(\emptyset, \varphi_t)$ are of non-linear nature with incorporation of the roll and turret motions. Similarly, the matrix $\mathrm{B(X, \theta, V_y, \varphi_{y,} T_{de}, T_{da})}$ is dependent upon the vehicle responses and input drive torques.